Synthesis, *in silico* study (DFT, ADMET) and crystal structure of novel sulfamoyloxy-oxazolidinones: Interaction with SARS-CoV-2

Abdeslem Bouzina[a], Malika Berredjem[a,*], Sofiane Bouacida[b,c], Khaldoun Bachari[d], Christelle Marminon[e], Marc Le Borgne[e], Zouhair Bouaziz[f], Yousra Ouafa Bouone[a]

[a] *Department of Chemistry, Laboratory of Applied Organic Chemistry, Synthesis of Biomolecules and Molecular Modelling Group, Sciences Faculty, Badji-Mokhtar-Annaba University, Box 12, Annaba 23000, Algeria*
[b] *Unité de Recherche de Chimie de L'Environnement et Moléculaire Structurale, Université des Fréres Mentouri, Constantine 25000, Algeria*
[c] *Département des Sciences de La Matiére, Université Larbi Ben M'Hidi, Oum El Bouaghi 04000, Algeria*
[d] *Centre de Recherche Scientifique et Technique en Analyses Physico-Chimiques (CRAPC), BP384, Bou-Ismail, Tipasa RP 42004, Algeria*
[e] *Small Molecules for Biological Targets Team, Centre de Recherche en Cancérologie de Lyon, Centre Léon Bérard, CNRS 5286, INSERM 1052, Université Claude Bernard Lyon 1, Univ Lyon, Lyon 69373, France*
[f] *Faculté de Pharmacie-ISPB, EA 4446 Bioactive Molecules and Medicinal Chemistry, SFR Santé Lyon-Est CNRS UMS3453-INSERM US7, Université de Lyon, Université Lyon 1, CEDEX 8, Lyon 69373, France*

ARTICLE INFO

ABSTRACT

A new series of sulfamoyloxyoxazolidinone (SOO) derivatives have been synthesized and characterized by single-crystal X-ray diffraction, NMR, IR, MS and EA. Chemical reactivity and geometrical characteristics of the target compounds were investigated using DFT method. The possible binding mode between SOO and Main protease (Mpro) of SARS-CoV-2 and their reactivity were studied using molecular docking simulation. Single crystal X-ray diffraction showed that SOO crystallizes in a monoclinic system with P 2 1 space group. The binding energy of the SARS-CoV-2/Mpro-SOO complex and the calculated inhibition constant using docking simulation showed that the active SOO molecule has the ability to inhibit SARS-CoV2. We studied the prediction of absorption, distribution, properties of metabolism, excretion and toxicity (ADMET) of the synthesized molecules.

© 2022 Elsevier B.V. All rights reserved.

1. Introduction

Compounds containing sulfonamide moiety have attracted much attention owing to their superior biological propertie [1]; because in drug discovery, sulfonamide can be valuable analogue of sulfamate, carboxylic acid, urea, carbamate, thioamide and amide functional groups. It has the advantage in many cases to increase the potency of inhibition and decrease the toxicity [2]. A large number of sulfonamide derivatives have been reported to exibit potent biological activities such as antitumor [3], anticonvulsant [4], anti-hypoglycemic [5] and anti-mycobacterial [6]. Additionally, the sulfonamide derivatives demonstrate promising value in the development of enzyme inhibitors including carbonic anhydrase I [7], HIV-1 protease [8], AChE inhibitory [9], metallocarboxypeptidase [10] and beta-3 adrenergic agonists [11].

The introduction of oxazolidinones moiety on sulfonamide has been widely studied, some of these studies have shown that sulfamoyloxazolidinones represent a very interesting class of compounds due to their various pharmacological activities [12].

Sulfamoyloxazolidinones are still the subject of research today in the medical field, such as compound **1** has shown modest efficacy against several strains of bacteria [13], compounds **2** and **3** show better antibacterial activity [14,15]. Where the oxazolidinone motif **4** is crucial for enhancing the inhibitory activity of HIV-1 as shown by a study carried out by Amin et al. [16].

On the other hand, viral infections have become a serious medical problem around the world, new infections continue to emerge today, and old ones are still rife, as shown by the epidemic of Severe Acute Respiratory Syndrome (SARS) and more recently Coronavirus disease 2019 (COVID-19) [17]. A disease which has severely crippled the entire world with the rise of more than 2000,000 confirmed cases across the global, and a death toll exceeding 170,000. This global pandemic Covid-19 touches every aspect of people's lives including one's health, education,…etc.

In the current spread of novel coronavirus (SARS-CoV-2), antiviral drug discovery is of great importance, until now, no potential and specific therapeutic agents is approved or available

---

* Corresponding author.
  E-mail address: angberredjem@yahoo.fr (M. Berredjem).

[18]. There's naturally an on-going, many researchers and scientists around the world being engaged in developing specific and potential antiviral drug to treat the SARS-CoV-2 infection [19,20]. The binding affinity and structure of protein-drug complexes play an important role in understanding the molecular mechanism in drug discovery. Moreover, the SARS-CoV-2 main protease is a key target for COVID-19 drug discovery. All *in silico* studies carried out on inhibitors which block SARS-CoV-2 replication by inhibition of main protease would be effective and specific measures for the development of new therapeutic agents against SARS-CoV-2 [21–27].

In continuation to our research [28] in the field of the synthesis of sulfonamide and oxazolidinone derivatives, we report here the synthesis and computational study of ten new sulfamoyloxazolidinone derivatives on the inhibitory potential of these new molecules against the main protease (M pro: **5R80**) of SARS-CoV-2. Optimization of absorption, distribution, metabolism, excretion and toxicity (ADMET) properties has been performed.

2. Materials and methods

2.1. Chemistry

2.1.1. Chemical methods

All chemicals and solvents were purchased from common commercial sources and were used as received without any further purification. All reactions were monitored by TLC on silica Merck 60 F_{254} percolated aluminum plates and were developed by spraying with ninhydrin solution (10% in EtOH). Column chromatography was performed with Merck silica gel (230–400 mesh). Proton nuclear magnetic resonance (^{1}H NMR) spectra were recorded on a Brücker spectrometer at 400 MHz. Chemical shifts are reported in δ units (ppm) with TMS as reference (δ 0.00). All coupling constants (J) are reported in Hertz. Multiplicity is indicated by one or more of the following: s (singlet), d (doublet), t (triplet), q (quartet), m (multiplet), sb (singlet board), dd (doublet of doublet), dtd (doublet of triplet of doublet). Carbon nuclear magnetic resonance (^{13}C NMR) spectra were recorded on a Brücker at 100 MHz. Chemical shifts are reported in δ units (ppm) relative to CDCl$_3$ or DMSO (δ 77.0 and 39.0–40.0). Infrared spectra were recorded on a Perkin Elmer 600 spectrometer. The purity of the final compounds (greater than 95%) was determined by uHPLC/MS on an Agilent 1290 system using a Agilent 1290 Infinity ZORBAX Eclipse Plus C18 column (2.1 mm × 50 mm, 1.8 μm particle size) with a gradient mobile phase of H$_2$O/CH$_3$CN (90:10, v/v) with 0.1% of formic acid to H$_2$O/CH$_3$CN (10:90, v/v) with 0.1% of formic acid at a flow rate of 0.5 mL/min, with UV monitoring at the wavelength of 254 nm with a run time of 10 min. Microanalysis spectra were performed by Elemental Analyser (Euro E.A. 3000-V3.0-single-2007), and the determined values were within the acceptable limits of the calculated values. Melting points were recorded on a Büchi B-545 apparatus in open capillary tubes.

2.1.2. General procedure for the synthesis of sulfamoyloxy-oxazolidinones C(1–10)

A solution of oxazolidinone (1 equiv) in anhydrous CH$_2$Cl$_2$ (5 mL) was added to a stirring solution of chlorosulfonylisocyanate (CSI) (1.1 equiv) in (5 mL) of anhydrous CH$_2$Cl$_2$ at 0 °C dropwise over a period of 30 min. The resulting solution was transferred to a mixture of primary or secondary amine (1.0 equiv) in CH$_2$Cl$_2$ (5 mL) in the presence of triethylamine (1.3 equiv). The solution was stirred at 0 °C for less than 1.5 h. The reaction mixture was washed with HCl 0.1 N and water, and the organic layer was dried over anhydrous sodium sulfate, filtered and concentrated in vacuo. The residue was purified by silica gel chromatography; or (9/1) mixture of diethyl ether and ethanol was added to the reaction mixture and pure product was crystallized to 6 °C overnight to give sulfamoyloxazolidinone-carboxamides in excellent yields.

(S)−4-benzyl-2-oxo-N-(N-phenylsulfamoyl)oxazolidine-3-carboxamide (Table 1, entry 1C). Cristal (88%); m.p. 132–134 °C. IR (KBr, cm^{-1}): 3284.19, 3142.33, 1741.30, 1357.87, 1160.90, 1028; ^{1}H NMR (400 MHz, CDCl$_3$): δ = 2.58 (dd, 1H, J_1 = 8, J_2 = 16 Hz, **CH$_2$**_CH*), 2.64 (dd, 1H, J_1 = 8, J_2 = 16 Hz, **CH$_2$**_CH*), 3.79–3.88 (m, 2H, **CH$_2$**_O), 4.10–4.17 (m, 1H, **CH***-N), 6.27 (s, 1H, **NH**-SO$_2$), 6.93–7.08 (m, 10H, **H**-Ar), 8.68 (s, 1H, **NH**−C = O); ^{13}C NMR (100 MHz, CDCl$_3$): δ = 41.02, 53.71, 69.57, 119.84, 120.66, 121.53, 127.02, 129.06, 129.25, 135.88, 136.37, 151.68, 160.21; Ms (m/z): 376.1 [M + 1]; Anal. Calc. for C$_{17}$H$_{17}$N$_3$O$_5$S: C, 54.39; H, 4.56; N, 11.19; S, 8.54; Found: C, 54.45; H, 4.63; N, 11.26; S, 8.60.

(S)−4-isopropyl-2-oxo-N-((4-phenylpiperazin-1-yl)sulfonyl) oxazolidine-3-carboxamide (Table 1, entry 2C). Cristal (83%); m.p. 136–138 °C. IR (KBr, cm^{-1}): 3258, 1750, 1725, 1344, 1154; ^{1}H NMR (400 MHz, CDCl$_3$): δ = 0.80 (t, 3H, J = 5.62 Hz, **CH$_3$**_CH), 0.84 (t, 1H, J = 5.64 Hz, **CH$_3$**_CH), 1.57–1.61 (m, 1H, **CH**$_{isop}$), 2.15–2.20 (m, 1H, **CH***), 3.30–3.33 (m, 4H, 2 **CH$_2$**_N), 3.40–3.54 (m, 4H, 2 **CH$_2$**_N), 3.96–4.42 (td, 2H, J_1 = 4.80, J_2 = 7.56, J_3 = 9.20 Hz, **CH$_2$**_O), 7.20–7.25 (m,5, **H**-Ar), 10.47 (s, 1H, **NH**−C = O); ^{13}C NMR (100 MHz, CDCl$_3$): δ = 14.61, 17.83, 28.55, 46.67, 49.49, 58.56, 64.37, 117.10, 124.14, 130.00, 147.50, 150.55, 155.69; Ms (m/z): 397.1 [M + 1]; Anal. Calc. for C$_{17}$H$_{24}$N$_4$O$_5$S: C, 51.50; H, 6.10; N, 14.13; S, 8.09; Found: C, 51.45; H, 6.17; N, 14.16; S, 8.15.

N-((3,4-dihydroisoquinolin-2(1H)-yl)sulfonyl)−2-oxooxazolidine-3-carboxamide (Table 1, entry 3C). Cristal (90%); m.p. 135–137 °C. IR (KBr, cm^{-1}): 3194.64, 1745.87, 1723.69, 1367.37, 1172.41; ^{1}H NMR (400 MHz, CDCl$_3$): δ = 2.96 (t, 2H, J = 5.9 Hz, **CH$_2$**-Ar), 3.72 (t, 2H, J = 5.9 Hz, **CH$_2$**_N), 4.00 (t, 2H, J = 8.1 Hz, **CH$_2$**_N), 4.47 (t, 2H, J = 5.9 Hz, **CH$_2$**_O), (s, 2H, Ar-**CH$_2$**_N), 7.08–7.11 (m, 1H, **CH**-Ar), 7.13–7.17 (m, 1, **H**-Ar), 7.17–7.21 (m, 2, **H**-Ar), 10.28 (s, 1H, **NH**−C = O); ^{13}C NMR (100 MHz, DMSO): δ = 20.99, 42.06, 44.65, 47.70, 62.87, 126.43, 126.59, 126.98, 128.97, 131.74, 133.48, 147.54, 155.21; Ms (m/z): 326.1 [M + 1]; Anal. Calc. for C$_{13}$H$_{15}$N$_3$O$_5$S: C, 47.99; H, 4.65; N, 12.92; S, 9.85; Found: C, 47.92; H, 4.62; N, 12.95; S, 9.88.

(S)−4-isobutyl-2-oxo-N-((4-phenylpiperazin-1-yl)sulfonyl)oxazolidine-3-carboxamide (Table 1, entry 5C). Cristal (94%); m.p. 140–142 °C. IR (KBr, cm^{-1}): 3193.50, 1753.78, 1721.00, 1370.20, 1173.10; ^{1}H NMR (400 MHz, CDCl$_3$): δ = 0.90 (d, 3H, J = 7.9 Hz, **CH$_3$**_CH), 0.92 (d, 3H, J = 7.8 Hz, **CH$_3$**_CH), 1.45–1.49 (m, 1H, **CH$_2$**), 1.51–1.59 (m, 1H, **CH$_2$**), 1.82–1.89 (m, 1H, **CH**$_{ispr}$), 3.16–3.22 (m, 4H, 2**CH$_2$**_N), 3.40–3.60 (m, 4H, 2**CH$_2$**_N), 4.13–4.16 (m, 1H, **CH***), 4.26 (dd, 1H, J_1 = 5.4, J_2 = 9.8, Hz, **CH$_2$**_O), 4.36–4.38 (m, 1H, **CH$_2$**_O), 6.86–6.90 (m, 2H, **H**-Ar), 7.22–7.27 (m, 2, **H**-Ar), 10.55 (s, 1H, **NH**−C = O); ^{13}C NMR (100 MHz, CDCl$_3$): δ = 14.62, 17.85, 28.56, 41.60, 46.74, 49.36, 64.37, 68.57, 117.02, 120.96, 124.40, 147.38, 150.77, 155.35; Ms (m/z): 397.3 [M + 1]; Anal. Calc. for C$_{17}$H$_{23}$N$_3$O$_5$S: C, 53.53; H, 6.08; N, 11.02; S, 8.40; Found: C, 53.69; H, 6.12; N, 11.05; S, 8.36.

(S)−4-benzyl-2-oxo-N-((4-phenylpiperazin-1-yl)sulfonyl)oxazolidine-3-carboxamide (Table 1, entry 6C). Cristal (91%); m.p. 139–141 °C. IR (KBr, cm^{-1}): 3186.20, 1754.34, 1723.16, 1362.12, 1167.24; ^{1}H NMR (400 MHz, CDCl$_3$): δ = 2.90 (dd, 1H, J_1 = 8, J_2 = 16 Hz, **CH$_2$**_CH*), 3.29–3.33 (m, 4H, 2 **CH$_2$**_N), 3.36 (d, 1H, J = 8 Hz, **CH$_2$**_CH*), 3.63–3.66 (m, 4H, 2 **CH$_2$**- N), 4.25–4.36 (m, 2H, **CH$_2$**_O), 4.46–4.71 (m, 1H, **CH***-N), 6.93–6.90 (m, 3H, **H**-Ar), 7.18–7.34 (m, 3H, **H**-Ar), 10.34 (s, 1H, **NH**−C = O); ^{13}C NMR (100 MHz, CDCl$_3$): δ = 38.11, 46.69, 49.63, 55.04, 67.23, 117.22, 127.75, 128.24, 129.47,

Table 1
Prepared sulfamoyloxy-oxazolidinones derivatives.

Comp code	Structure	Yield(%)	Comp code	Structure	Yield(%)
1C		88	6C		91
2C		83	7C		92
3C		90	8C		90
4C		92	9C		88
5C		94	10C		92

129.51, 134.43, 147.55, 155.15; Ms (*m/z*): 445.1 [*M* + 1]; Anal. Calc. for C$_{21}$H$_{24}$N$_4$O$_5$S: C, 56.74; H, 5.44; N, 12.60; S, 7.21; Found: C, 56.81; H, 5.48; N, 12.53; S, 7.27.

(S)−4-isopropyl-N-(morpholinosulfonyl)−2-oxooxazolidine-3-carboxamide (Table 1, entry 7C). White powder (92%); m.p. 143–145 °C. IR (KBr, cm^{-1}): 3284.19, 1741.43, 1357.87, 1160.90; ^{1}H NMR (400 MHz, CDCl$_3$): δ= 0.91(d, 3H, *J* = 12 Hz, **CH$_3$**-CH), 0.95 (d, 3H, *J* = 11.80 Hz, **CH$_3$**-CH), 1.67 (m, 1H, **CH**-$_{isop}$), 2.42–2.48 (m, 1H, **CH***-N), 3.41–3.42 (m, 4H, 2 **CH$_2$**-N), 3.74–3.79 (m, 4H, 2 **CH$_2$**-O), 3.36–3.44 (dd, 2H, *J$_1$* = 6.00, *J$_2$* = 12.00 Hz,**CH$_2$**-CH*), 10.35 (s, 1H, N**H**−C = O); ^{13}C NMR (100 MHz, CDCl$_3$): δ= 14.65, 17.88, 17.89, 18.15, 28.61, 46.80, 58.62, 64.41, 66.40, 147.57, 155.68; Ms (*m/z*): 322.1 [*M* + 1]; Anal. Calc. for C$_{11}$H$_{19}$N$_3$O$_6$S: C, 41.11; H, 5.96; N, 13.08; S, 9.98; Found: C, 41.17; H, 5.92; N, 13.02; S, 9.94.

(S)-N-((3,4-dihydroisoquinolin-2(1H)-yl)sulfonyl)−4-isopropyl-2-oxooxazolidine-3-carboxamide (Table 1, entry 8C). Cristal (90%); m.p. 148–150 °C. IR (KBr, cm^{-1}): 3248.39, 1747.91, 1366.67, 1162.52; ^{1}H NMR (400 MHz, CDCl$_3$): δ= 0.83 (d, 3H, *J* = 6.90 Hz, **CH$_3$**-CH), 0.88 (d, 1H, *J* = 7.1 Hz, **CH$_3$**-CH), 2.32 (dtd, 1H, *J$_1$* = 3.1, *J$_2$* = 6.9, *J$_3$* = 13.9 Hz, C**H***isp*), 2.97 (t, 2H, *J* = 7.1 Hz, **CH$_2$**-pH), 3.67–3.79 (m, 2H, **CH$_2$**-N), 4.25 (dt, 4H, *J$_1$* = 9.2, *J$_2$* = 7.9 Hz,

C**H***), 4.29–4.37 (m, 2H, **CH$_2$**-N), 4.62 (q, 2H, *J* = 15.7 Hz, **CH$_2$**-O), 7.07–7.22 (m, 4H, **H**-Ar), 10.38 (s, 1H, N**H**−C = O); ^{13}C NMR (100 MHz, CDCl$_3$): δ= 14.50, 14.69, 28.44, 28.68, 44.56, 47.68, 58.40, 64.21, 126.34, 126.50, 126.88, 128.85, 131.77, 133.37, 147.30, 155.20; Ms (*m/z*): 368.2 [*M* + 1]; Anal. Calc. for C$_{16}$H$_{21}$N$_3$O$_5$S: C, 52.30; H, 5.76; N, 11.44; S, 8.73; Found: C, 52.37; H, 5.72; N, 11.47; S, 8.71.

2-oxo-N-((4-phenylpiperazin-1-yl)sulfonyl)oxazolidine-3-carboxamide (Table 1, entry 9C). Cristal (88%); m.p. 119–121 °C. IR (KBr, cm^{-1}): 3186.5, 1743.99, 1716.0, 1368.4, 1171.1; ^{1}H NMR (400 MHz, CDCl$_3$): δ= 3.20–3.28 (m, 4H, 2**CH$_2$**-N-pH), 3.58–3.62 (m, 4H, 2**CH$_2$**-N-SO$_2$), 4.06 (dd, 2H, *J$_1$* = 8.9, *J$_2$* = 7.5, **CH$_2$**-N), 4.49 (dd, 2H, *J$_1$* = 8.8, *J$_2$* = 7.5 Hz, **CH$_2$**-O), 6.91–6.96 (m, 3H, **H**-Ar), 7.26–7.31 (m, 3H, **H**-Ar), 10.27 (s, 1H, N**H**−C = O); ^{13}C NMR (100 MHz, CDCl$_3$): δ= 42.10, 46.62, 49.51, 62.90, 117.14, 121.19, 129.43, 147.59, 150.48, 155.27; Ms (*m/z*): 355.1 [*M* + 1]; Anal. Calc. for C$_{14}$H$_{18}$N$_4$O$_5$S: C, 47.45; H, 5.12; N, 15.81; S, 9.05; Found: C, 47.51; H, 5.18; N, 15.85; S, 9.01.

(S)−4-benzyl-N-((3,4-dihydroisoquinolin-2(1H)-yl)sulfonyl)−2-oxooxazolidine-3-carboxamide ((Table 1, entry 10C). White powder (92%); m.p. 141–143 °C. IR (KBr, cm^{-1}): 3238.70, 1757.89, 1707.41, 1366.36, 1173.03; ^{1}H NMR (400 MHz, CDCl$_3$): δ= 2.82 (dd, 1H,

Table 2
Crystallographic data and refinement parameters for **6C**.

Formula	C$_{21}$ H$_{24}$ N$_4$ O$_5$S	Absorption coefficient (mm^{-1})	0.193
Formula weight	444.5	F(000)	936
Crystal habit, color	Prism, Colorless	Crystal size (mm)	0.55 × 0.40 × 0.12
Crystal system	Orthorhombic	θ range for data collection (°)	2.621 - 27.531
Space group	$P2_12_12_1$	Reflections collected	9825
a (Å)	5.3307(5)	Independent reflections	4528
b (Å)	14.4546(17)	R$_{int}$	0.0443
c (Å)	27.644(4)	Reflections with $I \geq 2\sigma(I)$	3274
α (°)	90	Number of parameters	281
β (°)	90	Goodness-of-fit on F^2	1.02
γ (°)	90	Final R indices [$I \geq 2\sigma(I)$]	R_1=0.0493, wR_2=0.080
Volume (Å^3)	2130.1(4)	R indices [all data]	R_1=0.0758, wR_2=0.0907
Z, Z'	4, 4	Largest difference peak and hole (Å^{-3})	0.251, −0.285
Density (calculated, g/cm^3)	1.386	CCDC deposition no.	CCDC 2,078,929
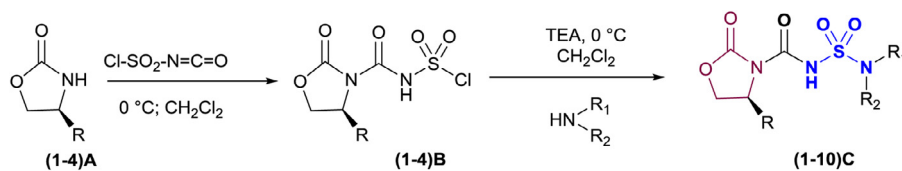
Scheme 1. Synthesis of sulfamoyloxy-oxazolidinones.
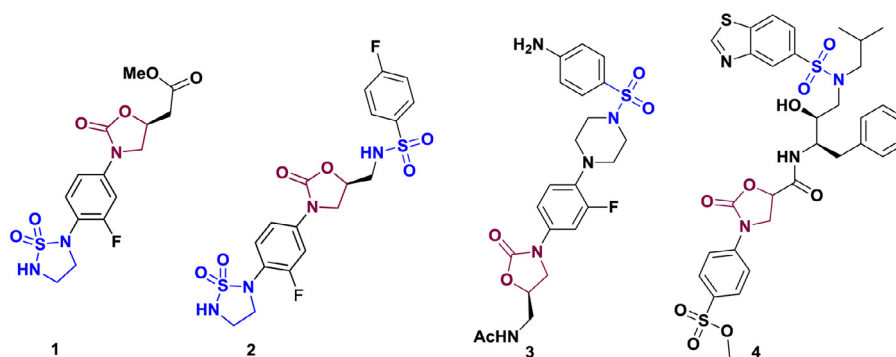
Fig. 1. Chemical structure of some sulfonamide approved drugs containing oxazolidinone cycle.
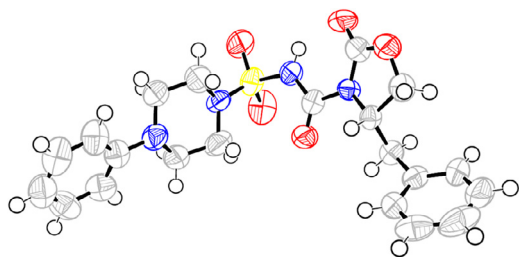
Fig. 2. Ortep diagram of compound **6C** displacement ellipsoids are drawn at the 50% probability level. H atoms are represented as small spheres of arbitrary radius.

J_1 = 13.5, J_2 = 9.1 Hz, **CH$_2$**-pH), 3.58–2.99 (t, 2H, J = 5.9 Hz, **CH$_2$**_CH$_2$_N), 3.21 (dd, J_1 = 13.6, J_2 = 3.2 Hz, 1H, **CH$_2$**-pH), 3.76 (t, J = 6.0 Hz, 2H,), 3.76 (t, 2H, J_1 = 6.0, **CH$_2$**_N), 4.18–4.33 (m, 2H, N−**CH$_2$**-pH), 4.55–4.73 (m, 3H, **CH$_2$**_O+**CH***), 7.08–7.34 (m, 9H, **H**-Ar), 10.34 (s, 1H, **NH**−C = O); ^{13}C NMR (100 MHz, CDCl$_3$): δ= 28.85, 38.04, 44.72, 47.80, 54.95, 67.18, 126.49, 126.67, 127.07, 127.71, 129.01, 129.20, 129.51, 131.87, 133.51, 134.49, 147.45, 155.12;
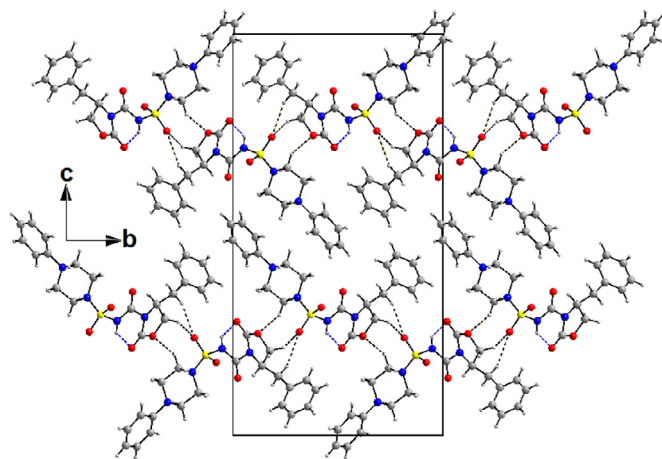
Fig. 3. Diagram packing of **6C** viewed along the a axis showing double layers parallel to (001), which are connected together with N-H...O (black dashed line) and C-H...O (blue dashed line) hydrogen bonds.

Table 3
Distances (Å) and angles (°) of hydrogen bond for **6C**.

D–H...A	d(D–H)	d(H...A)	d(D-A)	D–H–A	Symmetry
N3-H3A...O5	0.8800	1.9400	2.6483(4)	136.00	x,y,z
C8-H8A...O4	0.9900	2.5100	3.2432(5)	130.00	-x,−1/2 + y,1/2-z
C13- H13B...O1	0.9900	2.5100	3.2573(5)	132.00	1-x,1/2 + y,1/2-z
C15-H15B...O1	0.9900	2.5500	3.4056(5)	145.00	1-x,1/2 + y,1/2-z
C15-H15A...O3	0.9900	2.5400	3.0818(4)	114.00	x,y,z
C19-H19...Cg1 (C1-C6)	0.9900	2.85	3.6645(5)	144.00	$−1 + x$,1 + y,z

Table 4
Docking score and binding energy (kcal/mol) of synthesized sulfamoyloxy-oxazolidinones **C(1–10)** with the reference compound (Methyl 4-sulfamoylbenzoate) against SARS-CoV-2 main protease by molecular docking study.

Compound code	Glide Score	Binding Energy
1C	−7.807	−71.541
2C	−6.823	−62.212
3C	−6.785	−59.889
4C	−6.717	−60.256
5C	−6.682	−66.656
6C	−6.646	−61.193
7C	−6.486	−59.369
8C	−6.243	−58.532
9C	−6.074	−57.331
10C	−5.627	−51.038
Methyl 4-sulfamoylbenzoate	−6.551	−46.203
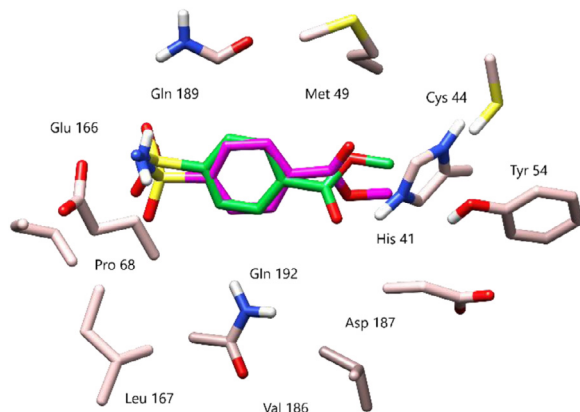
Fig. 4. Docked and co-crystalized methyl 4-sulfamoylbenzoate in the SARS-CoV-2 main protease after self-docking calculation.

Ms (*m/z*): 416.1 [*M* + 1]; Anal. Calc. for $C_{20}H_{21}N_3O_5S$: C, 57.82; H, 5.10; N, 10.11; S, 7.72; Found: C, 57.88; H, 5.17; N, 10.13; S, 7.74.

2.1.3. Crystallographic data

Crystallographic data for the studied compound (*S*)−4-benzyl-2-oxo-N-((4-phenylpiperazin-1-yl)sulfonyl)oxazolidine-3-carboxamide (**6C**) was collected on a Bruker APEX three-circle diffractometer equipped with an Apex II CCD detector using Mo-Kα (microfocus sealed tube with a graphite monochromator) radiation, at 150(2) K. The crystal was coated with Paratone oil and mounted on loops for data collection.

The crystallographic data and experimental details for structural analysis are summarized in (Table 2). The reported structure was solved by direct methods with SIR2002 [29] to locate all the non-H atoms which were refined anisotropically with SHELXL97 [30] using full-matrix least-squares on F2 procedure from within the WinGX [31] suite of software used to prepare material for publication. All absorption corrections were performed with the SAD-ABS program [32]. All non-hydrogen atoms were located in dif-ference Fourier maps and were refined anisotropically. Hydrogen atoms were placed in idealized geometrical positions and refined with Uisotied to the parent atom with the riding model.

CCDC 2,078,929, contain the supplementary crystallographic data for compound **6C**. These data can be obtained free of charge from The Cambridge Crystallographic Data centre via www.ccdc.cam.ac.uk/data_request/cif.

2.2. Computational methods

2.2.1. Molecular docking

The X-ray crystal structure of SARS-CoV-2 main protease (PDB ID: **5R80**) was obtained from the Protein Data Bank [33], and was prepared with Protein Preparation Wizard tool implemented in Schrodinger suite, assigning bond orders, adding hydrogens and optimizing H-bonding networks. The three-dimensional structures of the derivatives were constructed using Maestro software, and prepared with Ligprep using Optimized Potentials for Liquid Simulation (OPLS3e) force field with a convergence of heavy atoms of 0.30 Å [34]. The Grid was centered on the centroid of the co-crystallized ligand (Methyl 4-sulfamoylbenzoate).

The final prepared PDB file of the protein and synthesized N-acylsulfamoyloxazolidinones **C(1–10)** were submitted in order to run docking process. Docking studies were performed by Glide software [35] at Extra Precision [36]. Output files of Methyl 4-sulfamoylbenzoate and docked compounds along with SARS-CoV-2 main protease protein were visualized on Chimera software.

2.2.2. Density functional theory (DFT) analysis

Molecular geometry the gas phase structure optimization of sulfamoyloxy-oxazolidinones derivatives (**1–10)C** is optimized using DFT at B3LYP method [37,38], with the basis set of 6–31 G (d,p) implemented by Gaussian 09 package [39,40]. Frontier molecular orbitals and global reactivity descriptors the highest occupied molecular orbital (HOMO) and lowest unoccupied molecular orbital (LUMO) [41], energy gap and chemical reactivity descriptors are calculated at DFT/B3LYP/6-31 G (d, p) method.

3. Results and discussion

3.1. Synthesis

Recently, a great deal of research has been devoted to the synthesis and development of new sulfamides [42], the synthesis of these compounds has an important place in the perspective of interfering with biological processes and discover of new drugs [43].

In this context we were interested to prepare a new series of sulfamide containing the oxazolidinone moiety.

The synthetic route for the preparation of sulfamoyloxy-oxazolidinones (**1–10)C** is outlined in Scheme 1.

The synthesis was carried out in two steps [44]. First, carbamoylation under anhydrous conditions of commercial chloro-sulfonyl isocyanate with the corresponding oxazolidinones (**1–4)A**, easily prepared in a two-step quantitatively afforded the corresponding N-chlorosulfonyl carbamate intermediate (**1–4)B**.

Table 5

Analysis of binding interaction of synthesized sulfamoyloxy-oxazolidinones **C(1–10)** with the reference compound against SARS-CoV-2 main protease.

Compound	Hydrogen bond	Hydrophobic interaction
1C	**Glu166**, Gly143, Asn142	Met49, Met165, Leu141, Pro52, Cys145
2C	**Glu166**, Gln189, Thr190, Gln192	Met49, Met165, Leu167, Pro168, Cys44
3C	**Glu166**, Gly143, Asn 142	Met49, Met165, Leu167, Pro168, Cys145
4C	**Glu166**	Met49, Met165, Leu167, Pro168, Cys44, Val186
5C	**Glu166**, Gln189, Thr190, Gln192	Met49, Met165, Leu167, Pro168, Cys44
6C	**Glu166**, Gln189, Thr190, Gln192	Met49, Met165, Leu167, Pro168, Cys44, Val186
7C	**Glu166**	Met49, Met165, Leu167, Pro168, Cys44, Val186, Cys145
8C	**Glu166**	Met49, Met165, Leu27, Pro152, Cys44, Tyr54, Cys145
9C	Gly143, Ser144, Cys145	Met49, Met165, Leu141, Pro168, Cys44, Phe140
10C	Asn142	Met49, Met165, Leu167, Pro168, Cys44, Val, Tyr54, Cys145
Methyl 4-sulfamoylbenzoate	**Glu166**	Met49, Met165, Leu167, Pro168, Cys44, Val186

Table 6

The HOMO, LUMO energies and band gap of synthesized compounds **C(1–10)**.

Molecular descriptors	Gas phase									
	1C	2C	3C	4C	5C	6C	7C	8C	9C	10C
Log P	2.20	2.11	0.79	2.34	2.46	2.90	−0.12	1.99	0.91	2.78
μ (D)	3.5487	4.8410	3.6544	3.4043	3.0961	5.9158	4.4372	5.4240	4.4372	4.3885
E_{HOMO}	−6.4553	−5.6025	−6.7340	−6.5791	−5.4267	−6.6567	−5.5073	−6.6567	−5.5073	−6.6640
E_{LUMO}	−0.0182	−0.7453	−1.7616	−0.7855	−0.8176	−0.8519	−0.6342	−0.7344	−0.9208	−0.8231
ΔE_{gap}	6.4371	4.8572	4.9724	5.7936	4.6091	5.8048	4.8731	5.9223	**4.5865**	5.8409
(η)	3.2185	2.4286	3.7005	2.8968	2.3045	2.9024	2.4370	2.9611	2.2933	2.9204
(S)	0.3107	0.4117	0.2702	0.3452	0.4339	0.3445	0.4103	0.3377	0.4360	0.3424
(μ)	−3.2367	−3.1739	−4.2478	−3.6823	−3.1221	−3.7543	−3.0707	−3.5966	−3.2140	−3.7435
(χ)	3.2367	3.1739	4.2478	3.6823	3.1221	3.7543	3.0707	3.5966	3.2140	3.7435
(ω)	1.6275	2.0739	2.4380	2.3409	2.1148	2.4281	1.9345	2.1842	2.2521	2.3992

Electronegativity (χ) = - (E_{HOMO} + E_{LUMO})/2, Electronic Chemical Potential (μ) = -χ = (E_{HOMO} + E_{LUMO})/2, Chemical Hardness (η) = (E_{LUMO} - E_{HOMO})/2, Electrophilicity Index (ω) = μ^2/2η, molecular softness (S) = 1/η.
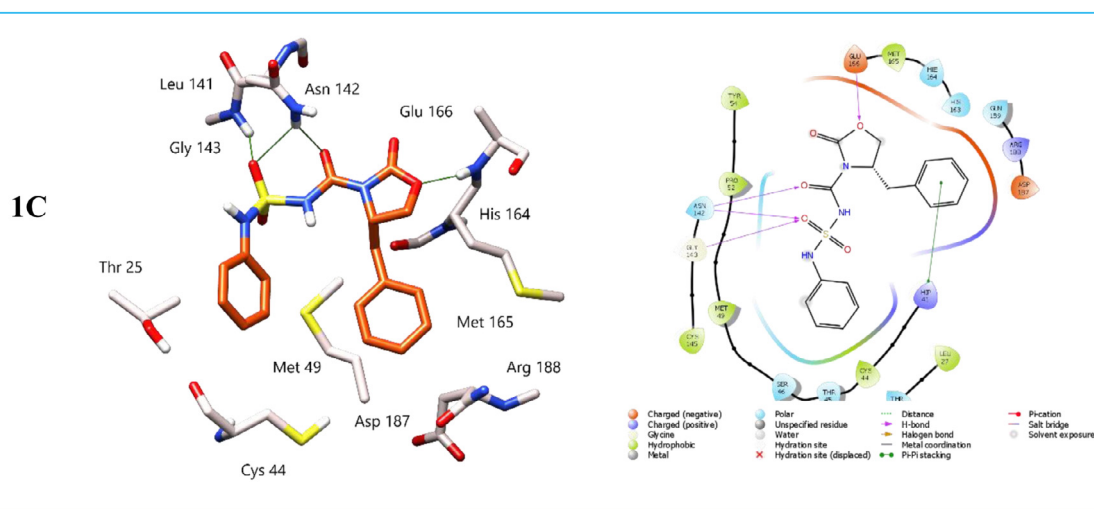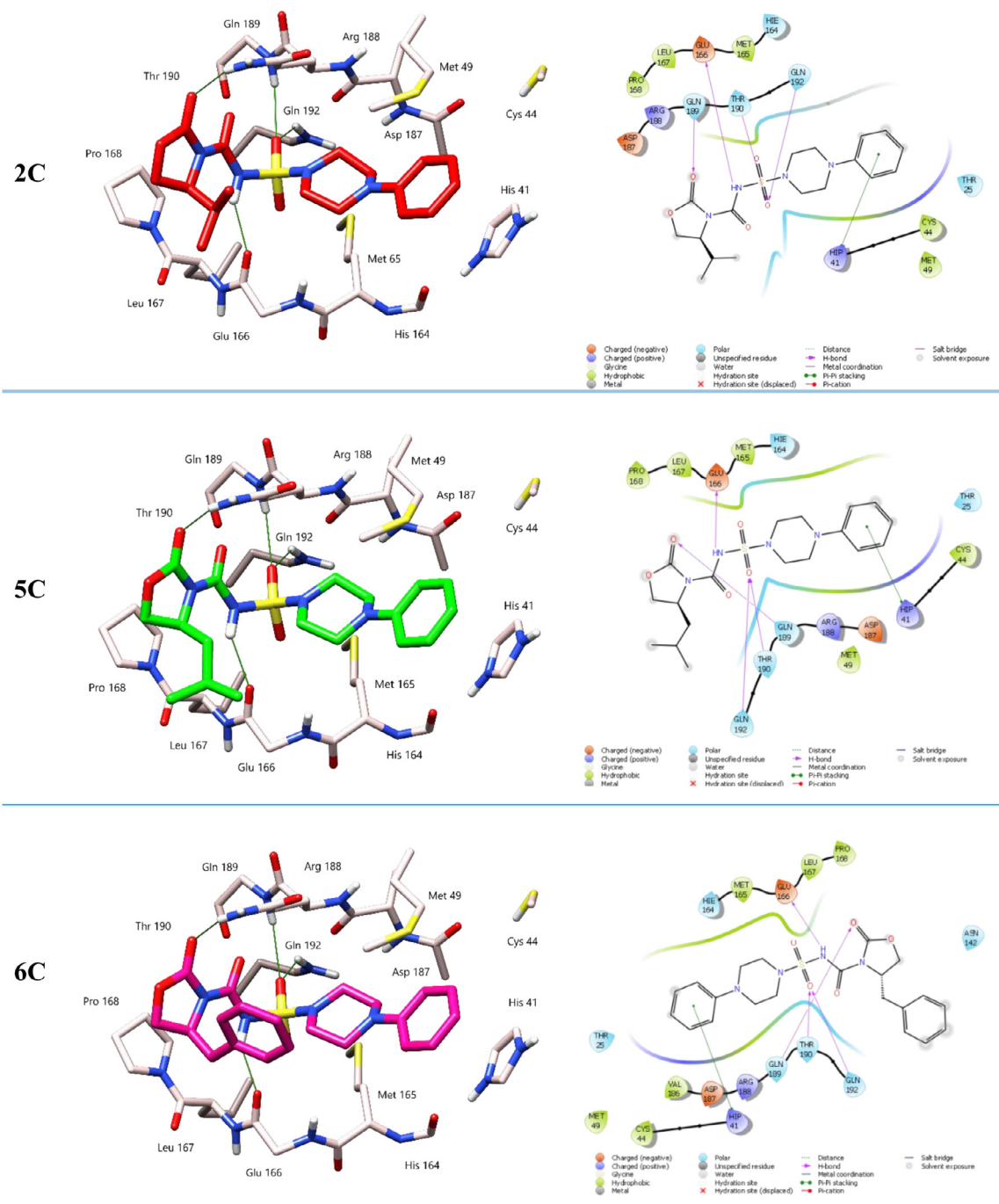

Fig. 5. 3D left and 2D right binding disposition of compound **1C** after docking calculations in the active site of SARS-CoV-2 main protease. The amino acid residues were shown as stick model and H-bonds were shown as green lines.

Scheme 1 Reaction with various primary or secondary amines in the presence of triethylamine at 0 °C then gave the target compounds **(1–10)C** in excellent yields (92–99%) within 60-90 min.

The structures of the synthesized sulfamoyloxy-oxazolidinones **C(1–10)** are presented in Table 1.

The structures of the prepared compounds **C(1–10)** were confirmed by spectroscopic methods (^{1}H, ^{13}C, HMBC, and HSQC) NMR, IR, EA, and X-ray analysis (Fig. 2). The purity of the final compounds was determined by uHPLC/MS on an agilent 1290 system. The results are presented in the experimental section. The FT-IR spectrum showed the characteristic signals of the three functions, namely the carbamate NH stretching at 3284–3186 cm^{-1} and its

C = O stretching at 1741-1707 cm^{-1}, the carbonyl of oxazolidinone group at 1757–1741 cm^{-1}, and the sulfamide group with its two signals at 1370–1344 cm^{-1} and 1173–1154 cm^{-1}. The molecular peak [M + H]$^+$ obtained by LC-MS was always present and corresponded to each synthesized compound. NMR spectra were recorded using CDCl$_3$ as the solvent and are available in the supplementary material part. The ^{1}H spectrum always exhibited a dramatically singlet at 8.68–10.55 ppm corresponding to the N−H proton. The ^{13}C spectrum was also characteristic due to the peaks related to the presence of two carbonyls at 147.30–151.61 ppm and 155.15–160.21 ppm confirm the formation of the sulfamoyloxy-oxazolidinones.

Fig. 6. 3D left and 2D right binding disposition of compounds **2C**, **5C** and **6C** after docking calculations in the active site of SARS-CoV-2 main protease. The amino acid residues were shown as stick model and H-bonds were shown as green lines.

3.2. Crystal characterization

Structural resolution revealed that the asymmetric unit consists of one molecule of (*S*)−4-benzyl-2-oxo-N-((4-phenylpiperazin-1-yl)sulfonyl)oxazolidine-3-carboxamide (**6C**), which crystallizes in the orthorhombic crystal system with $P2_12_12_1$ space group (Table 2).

The ORTEP diagram of this compound is shown in (Fig. 2).

The dihedral angle between the mean planes of the two phenyl rings is 73.37(1)°.

The crystal packing can be described as alternating double layers parallel to (001) plane at $c = 1/4$ and $c = 3/4$ along c axis. Which are connected together with N−H...O and C−H...O inter- and intra- molecular hydrogen bonds along the b axis (Fig. 3, Table 3). Based on the connectivity of these interactions, we have formation of chains and rings, respectively, with $C_1^1(8)$, $C_2^2(17)$, $R_4^4(25)$ and $R_6^6(41)$ graph-set motifs, leading a three-dimensional molecular structure. The crystal structure is also supported by intermolecular interactions of C−H... π (Table 3).
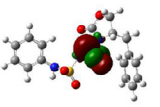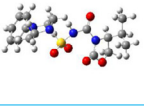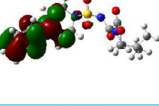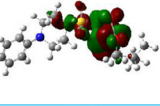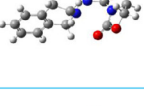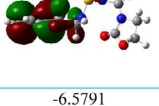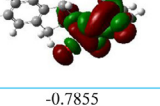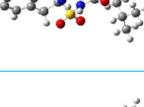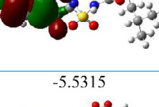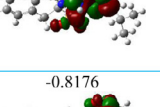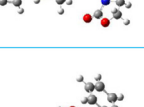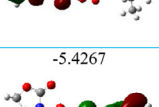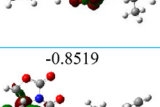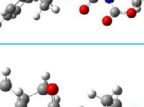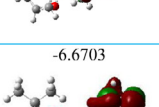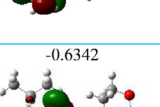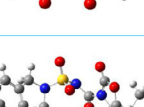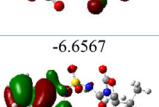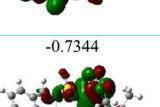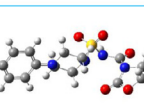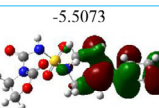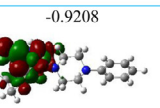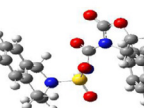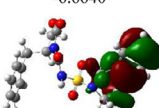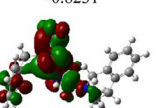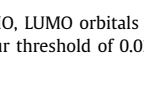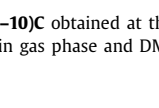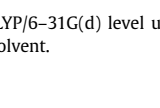
Comp	Optimized structure	HOMO	LUMO
1C		-6.4553	-0.0182
2C		-5.6025	-0.7453
3C		-6.7340	-1.7616
4C		-6.5791	-0.7855
5C		-5.5315	-0.8176
6C		-5.4267	-0.8519
7C		-6.6703	-0.6342
8C		-6.6567	-0.7344
9C		-5.5073	-0.9208
10C		-6.6640	-0.8231

Fig. 7. HOMO, LUMO orbitals for **(1–10)C** obtained at the B3LYP/6–31G(d) level using a contour threshold of 0.02 a.u in gas phase and DMSO solvent.

In these layers, the arrangement of each molecule induces a $\pi-\pi$ staking intramolecular interactions. The distance centroid–centroid is 4.9476(7)Å between phenyl rings not in the same asymmetric unit (with translation of $1 + x, -1 + y, z$) [45,31].

3.3. Molecular docking

In order to understand the interactions between protein and ligand, molecular docking study was performed to explore the binding mode of the prepared sulfamoyloxy-oxazolidinones to the SARS-CoV-2 main protease we have performed our studies using Schrodinger suite (version 11.8) and UCSF Chimera (version 1.13.1)

programs, and the Methyl 4-sulfamoylbenzoate was taken as reference ligand to investigate the binding mode of the studied synthesized derivatives **C(1–10).**

Accuracy of docking protocol was examined by re-docking of Methyl 4-sulfamoylbenzoate in the active site of SARS-CoV-2 main protease. Fig. 4 shows docked Methyl 4-sulfamoylbenzoate and co-crystallized one in almost same position among the receptor (RMSD = 0.84 Å) that confirmed validation of docking protocol using Extra Precision scoring function, in absence of water molecules.

The results of this study including the estimated glide score of the docked positions are provided in Table 4. Molecular docking study of all compounds revealed compounds (**1C, 2C, 3C, 4C, 5C, 6C, 7C, 8C** and **9C**) found to be stable inside the cavity among the 10 synthesized derivatives.

Compounds **1C, 2C, 3C, 4C, 5C** and 6C gave a better glide score in the range (−7.807 to −6.646 kcal/mol) when compared with the reference compound, with binding score of −6.551 kcal/mol.

Analysis of the molecular docking results showed that the interactions within the active site of SARS-CoV-2 main protease were attributed to hydrogen bonds, hydrophobic and electrostatic attraction forces. The docking results of the synthesized compounds and Methyl 4-sulfamoylbenzoate were reported in Table 5.

We have noticed that the stable compounds form a hydrogen bond with the Glu166 residue as the binding of the reference ligand; these compounds also form other important hydrogen bonds with the residues Gln192, Gln189, Gly143, Asn142.

Compound **1C**, which has the least docking score (−7.807 kcal/mol) is most favorable, with the most interesting interaction inside the pocket. This compound formed 4 hydrogen bonds, the first one between the doublet of oxygen atom of oxazolidinone and Glu166 residue, the second between the doublet of oxygen atom of sulfamide group and Gly143 residue, the third and the last hydrogen bonds formed between Asn42 residue and the sulfamoyloxy group. Moreover, it developed electrostatic attraction forces and two aromatic $\pi-\pi$ stacking interactions with Hip41 and His 41, which explains its great value of glide score and binding energy. (Fig. 5).

Also, **2C, 5C** and **6C** show significant stability in the active site with a docking score higher than the reference ligand, these compounds form important hydrogen bond with the Glu166 residue, as well as other hydrogen bonds with the Gln189, Thr190, Gln192 residues. In addition, theses compounds developed electrostatic attraction forces and aromatic $\pi-\pi$ stacking interactions with Hip41 and His 41 (Fig. 6).

Compounds **9C** and **10C** exhibited lower potency compared with others compounds and Methyl 4-sulfamoylbenzoate, because they lost the hydrogen bond with Glu166 as well as the electrostatic interactions with the amino acid residues in the active site.

Docking analysis revealed that among 10 synthesized derivatives, 8 compounds interact with SARS-CoV-2 main protease in good manner and confirms the importance of presence the donor and acceptor moieties such as oxazolidinone and sulfamide.

3.4. DFT study

The molecular geometry of synthesized sulfamoyloxy-oxazolidinones and the nature of their substituents are often correlated with their stability and their reactivity. In order to specify the relationship between the results of the molecular docking with the structure of the molecules and to evaluate this relationship, DFT study were carried out by Gaussian 09. This study gives some important and necessary information on the structure and reactivity of sulfamoyloxy-oxazolidinones.

The HOMO and LUMO (H–L) energy gap describes the chemical reactivity, kinetic stability and chemical softness of a molecule. The chemical reactivity descriptors estimated using DFT are chem-
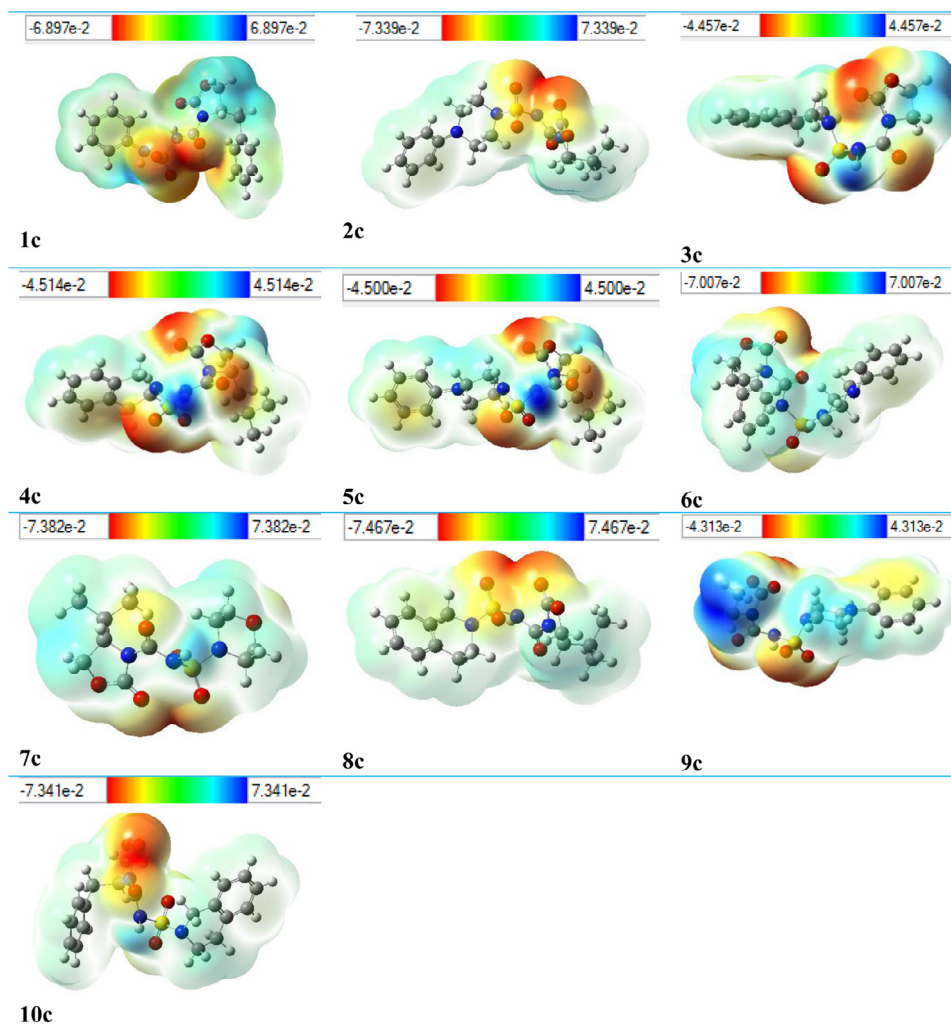
Fig. 8. MEP formed by mapping of total density over electrostatic potential in gas phase for all the synthesized compounds **(1–10)C.**

Table 7
Binding affinity and pharmacokinetic parameters of synthesized sulfamoyloxy-oxazolidinones.

Properties	1C	2C	3C	4C	5C	6C	7C	8C	9C	10C	Beclabuvir
Molecular weight (g/mole)	375.40	396.46	325.34	381.45	410.49	444.50	321.35	367.42	354.38	431.46	659.8
Rotatable bonds	7	6	4	6	7	7	5	5	5	6	6
H-bond donor	2	1	1	1	1	1	1	1	1	1	1
H-bond acceptor	5	6	6	6	6	6	7	6	6	7	7
Violations	0	0	0	0	0	0	0	0	0	0	**2**
Log Po/W iLogP	1.87	2.50	0.74	2.33	2.88	2.47	1.67	2.05	0.86	0.00	4.62
Log S ESOL	−4.25	−3.66	−2.47	−3.76	−3.90	−4.41	**−1.86**	−3.52	−2.61	−4.32	−6.95
GI	High	High	High	High	High	High	High	High	High	High	High
BBB	No	No	No	No	No	No	No	No	No	No	No
Log Kp	−6.11	−6.92	−7.52	−6.62	−6.75	−6.77	−7.86	−6.79	−7.65	−6.79	−6.55
Bioavailability Score	0.55	0.55	0.55	0.55	0.55	0.55	0.55	0.55	0.55	0.55	0.17
TPSA (˚A)	113.19	107.64	104.40	104.40	107.64	107.64	113.63	104.40	107.64	121.47	107.64

ical hardness (η), electronic chemical potential (μ), electronegativity (χ) and electrophilicity index (ω). The values of HOMO-LUMO gap, hydrophobicity coefficient Log p and the GCRD parameters are shown in Table 6 and Fig. 7.

Most of the studied compounds show a significant lipophilicity (Log p) in the range of [1.99–2.90] except the derivatives **3C, 9C** and **7C** which presents the lowest value of Log p= −0.12.

The compound **1C** has the highest energy gap $\triangle$Egap=6.4371, it is the most stable of all studied compounds; this value confirms

the results obtained by the molecular docking. The gap energy ($\triangle$Egap) of other compounds is in the range of [5.8409–4.5865].

The results show that the gap energy $\triangle$Egap is strictly proportional to the total energy (Table 6).

The 3D plot of the molecular electrostatic potential (MEP) has been established extensively as a useful quantity to explain hydrogen bonding, reactivity and structural activity of molecular behaviors. The negative regions represented by red and yellow colors are associated with electrophilic reactivity and positive regions rep-

Fig. 9. Radar related to physicochemical properties of molecules **1C-10C**.

resented by blue color are associated with nucleophilic reactivity. The color code of the map is in the range between 7.467 (deepest blue) and −7.341 (deepest red) (**Fig. 8**).

3.5. In silico *pharmacokinetics analysis of compound (1–10)C*

It is necessary to study the pharmacokinetic properties such as absorption, distribution, metabolism, excretion and toxicity (AD-MET) of any molecule classified as drug candidate, before pro-

ceeding to *in vivo* testing. The drug-likeness of synthesized compounds were predicted using ADME properties calculated from Swiss ADME. These fundamental parameters determine the resemblance to the drug as well as the activity inside the body of the studied substance [46].

The pharmacokinetic process of a drug answers whether a drug is able to get to the site of action. The pharmacodynamic process provides the answer of whether or not a drug is able to produce the required pharmacological effect.

The pharmacokinetic properties such as gastrointestinal absorption (GI), water soluble capability (Log S), lipophilicity (LogPo/W), CYP1A2 inhibitor and Blood Brain Barrier (BBB) are very important for any compound to be considered as a drug candidate [47].

Based on Lipinski's rule on orally active drug has a total number of hydrogen bond donors $\leq$ 5, hydrogen bond acceptors $\leq$ 10, logP $\leq$ 5, and molecular weight $<$ 500 da [48].

Analysis of Table 7 have revealed that all the studied compounds **C(1–10)** showed good gastrointestinal absorption (GI), they have consensus lipophilicity (LogPo/W) value in the range 0.74–2.88 and blood brain barrier (BBB) penetration properties, also their molecular weights are less of 500 da.

Table 7 and Fig. 9 show the *in silico* physicochemical properties, druglikeness, and pharmacokinetics of SOO compared with Beclabuvir as antiviral drug.

As shown in Fig. 9, all multifunctional sulfamoyloxyoxazolidinone had physicochemical profiles that makes them suitable for oral administration. All compounds had FLEX and POLAR (or TPSA) values that were inside the desired range for enhanced bioavailability (see shaded regions in Fig. 9).

Fig. 9 shows physicochemical property of possible oral drug candidates according to five different rules determined by the Lipinski, Ghose, Veber, Egan, and Muegge [49–52].

4. Conclusion

In the current study, 10 derivatives of novel sulfamoyloxyoxazolidinones were designed and synthesized. A structural elucidation of the new compounds was confirmed using spectroscopy and spectrometry methods (IR, LC-MS, NMR and EA). The prepared compounds were optimized using DFT-B3LYP method and 6-31 G (d, p) level. The predicted geometrical parameters of synthesized compounds agreed well with the experimental findings. The results of molecular docking study of the synthesized derivatives into the actives site of SARS-CoV-2 main protease revealed higher docking score and binding free energies for the study compounds compared with reference ligand. The results established the utility of the molecules as suitable candidates for the development of the new anti-SARS-CoV-2 agent.

Funding

Declaration of Competing Interest

All authors declare no conflict of interest.

CRediT authorship contribution statement

Abdeslem Bouzina: Investigation. **Malika Berredjem:** Writing – original draft, Conceptualization, Methodology, Writing – review & editing, Software. **Sofiane Bouacida:** Writing – review & editing. **Khaldoun Bachari:** Formal analysis. **Christelle Marminon:** Writing – review & editing. **Marc Le Borgne:** Writing – review & editing. **Zouhair Bouaziz:** Writing – review & editing. **Yousra Ouafa Bouone:** Investigation.

Acknowledgements

Supplementary materials

Supplementary material associated with this article can be found, in the online version, at doi:10.1016/j.molstruc.2022.132579.

References

[1] W. Spillane, J.B. Malaubier, Sulfamic acid and its N- and O-substituted derivatives, Chem. Rev. 114 (2014) 2507–2586, doi:10.1021/cr400230c.

[2] (a) G.A. Patani, E.J. LaVoie, Bioisosterism: a rational approach in drug design, Chem. Rev. 96 (1996) 3147–3176, doi:10.1021/cr950066q; (b) A.B. Reitz, G.R. Smith, M.H. Parker, The role of sulfamide derivatives in medicinal chemistry: a patent review (2006–2008), Expert Opin. Ther. Pat. 19 (2009) 1449–1453, doi:10.1517/13543770903185920.

[3] R. Crespo, M.G. de Bravo, P.A. Colinas, R.D. Bravo, *In vitro* antitumor activity of N-glycosyl sulfonamides, Bioorg. Med. Chem. Lett. 20 (2010) 6469–6471, doi:10.1016/j.bmcl.2010.09.052.

[4] M.L. Villalba, A.V. Enrique, J. Higgs, R.A. Castaño, S. Goicoechea, F.D. Taborda, L. Gavernet, I.D. Lick, M. Marder, L.E. Bruno Blanch, Novel sulfamides and sulfamates derived from amino esters: synthetic studies and anticonvulsant activity, Eur. J. Pharmacol. 774 (2016) 55–63, doi:10.1016/j.ejphar.2016.02.001.

[5] H. Berredjem, Y. Reggami, M. Benlaifa, M. Berredjem, N. Bouzerna, Antidiabetic and hypolipidemic potential of 3, 4-dihydroisoquinolin-2(1H)-sulfonamide in alloxan induced diabetic rats, Int. J. Pharm. 11 (2015) 226–235, doi:10.3923/ijp.2015.226.235.

[6] K. Suthagar, A.J. Fairbanks, Synthesis and anti-mycobacterial activity of glycosyl sulfamides of arabinofuranose, Org. Biomol. Chem. 14 (2016) 1748–1754, doi:10.1039/c5ob02317c.

[7] E. Berrino, S. Bua, M. Mori, M. Botta, V.S. Murthy, V. Vijayakumar, Y. Tamboli, G. Bartolucci, A. Mugelli, E. Cerbai, et al., Novel sulfamide-containing compounds as selective carbonic anhydrase I inhibitors, Molecules 22 (2017) 1049, doi:10.3390/molecules22071049.

[8] C.J. Bungard, P.D. Williams, J. Schulz, C.M. Wiscount, M.K. Holloway, H.M. Loughran, J.J. Manikowski, H.P. Su, D.J. Bennett, et al., Design and synthesis of piperazine sulfonamide cores leading to highly potent HIV-1 protease inhibitors, ACS Med. Chem. Lett. 8 (2017) 1292–1297 10.1021%2Facsmedchemlett.7b00386.

[9] R. Ulus, B.Z. Kurt, I. Gazioğlu, M. Kaya, Microwave assisted synthesis of novel hybrid tacrine-sulfonamide derivatives and investigation of their antioxidant and anticholinesterase activities, Bioorg Chem. 70 (2017) 245–255, doi:10.1016/j.bioorg.2017.01.005.

[10] N. Halland, J. Czech, W. Czechtizky, A. Evers, M. Follmann, M. Kohlmann, H.A. Schreuder, C. Kallus, Sulfamide as zinc binding Motif in small molecule inhibitors of activated thrombin activatable fibrinolysis inhibitor (TAFIa), J. Med. Chem. 59 (2016) 9567–9573, doi:10.1021/acs.jmedchem.6b01276.

[11] R. Kuang, J.B. Epp, S. Ruan, L.S. Chong, R. Venkataraman, J. Tu, S. He, T.M. Truong, W.C. Groutas, Utilization of the 1, 2, 5-thiadiazolidin-3-one 1, 1 dioxide scaffold in the design of potent inhibitors of serine proteases: SAR studies using carboxylates, Bioorg. Med. Chem. 8 (2000) 1005–1016, doi:10.1016/s0968-0896(00)00038-9.

[12] (a) M. Nessaib, M. Abdaoui, A. Djahoudi, M. Kadri, J.Y. Winum, Synthesis of substituted N-aryl-N-sulfamoyloxazolidin-2-ones with potential antibacterial activity, Recent Pat. Antiinfect. Drug Discov. 2 (2007) 131–139, doi:10.2174/157489107780832604; (b) Y. Bharath, G.R. Alugubell, R. Sreenivasulu, M.V. Basaveswara Rao, Design, synthesis of novel oxazolidino amides/sulfonamides conjugates and their impact on antibacterial activity, Chem. Pap. 72 (2018) 457–468, doi:10.1007/s11696-017-0298-1.

[13] (a) S.J. Kim, M.H. Jung, K.H. Yoo, J.H. Cho, C.H. Oh, Synthesis and antibacterial activities of novel oxazolidinones having cyclic sulfonamide moieties, Bioorg. Med. Chem. Lett. 18 (2008) 5815–5818, doi:10.1016/j.bmcl.2008.09.034; (b) C. Barbey, R. Bouasla, M. Berredjem, N. Dupont, P. Retailleau, N.E. Aouf, M. Lecouvey, Synthesis and structural study of new substituted chiral sulfamoyl oxazolidin-2-ones, Tetrahedron 68 (2012) 9125–9130, doi:10.1016/j.tet.2012.08.001; (c) F. Bouchareb, M. Berredjem, S.A. Kaki, A. Bouaricha, A. Bouzina, B. Belhani, N.E. Aouf, Synthesis and antibacterial activity of new chiral N-sulfamoyloxazolidin-2-ones, J. Chem. Sci. 128 (2016) 85–91, doi:10.1007/s12039-015-1004-x.

[14] A. Kamal, P. Swapna, V.C.R. Shetti, A.B. Shaik, M.P.N. Rao, S. Gupta, Synthesis, biological evaluation of new oxazolidino-sulfonamides as potential antimicrobial agents, Eur. J. Med. Chem. 62 (2013) 661–669, doi:10.1016/j.ejmech.2013.01.034.

[15] (a) A. Kamal, R.V.C. Shetti, S. Azeeza, P. Swapna, M.N.A. Khan, A.M. Reddy, I.A. Khan, S. Sharma, S.T. Abdullah, Anti-tubercular agents. Part 6: synthesis and anti-mycobacterial activity of novel arylsulfonamido conjugated oxazolidinones, Eur. J. Med. Chem. 46 (2011) 893–900, doi:10.1016/j.ejmech.2010.12.028; (b) A. Kamal, R.V.C. Shetti, S. Azeeza, S.K. Ahmed, P. Swapna, A.M. Reddy, I.A. Khan, S. Sharma, S.T. Abdullah, Anti-tubercular agents. Part 5: synthesis and biological evaluation of benzothiadiazine 1, 1-dioxide based congeners, Eur. J. Med. Chem. 45 (2010) 4545–4553, doi:10.1016/j.ejmech.2010.07.015.

[16] S.A. Amin, N. Adhikari, S. Bhargava, T. Jha, S. Gayen, Structural exploration of hydroxyethylamines as HIV-1 protease inhibitors: new features identified, SAR QSAR Environ. Res. 29 (2018) 385–408, doi:10.1080/1062936x.2018.1447511.

[17] (a) M.D. Segall, A.P. Beresford, J.M.R. Gola, D. Hawksley, M.H. Tarbit, Focus on success: using a probabilistic approach to achieve an optimal balance of compound properties in drug discovery, Expert Opin. Drug Metab. Toxicol. 2 (2006)

325–337, doi:10.1517/17425255.2.2.325; (b) S.P. Adhikari, S. Meng, Y.J. Wu, Y.P. Mao, R.X. Ye, Q.Z. Wang, C. Sun, S. Sylvia, S. Rozelle, H. Raat, H. Zhou, Epidemiology, causes, clinical manifestation and diagnosis, prevention and control of coronavirus disease (COVID-19) during the early outbreak period: a scoping review, Infect. Dis. Poverty 9 (2020) 1–12, doi:10.1186/s40249-020-00646-x.

[18] M.L. Sun, J.M. Yang, Y.P. Sun, G.H. Su, Inhibitors of RAS might be a good choice for the therapy of COVID-19 pneumonia, Chin. J. Tuberc. Respir. Dis. 43 (2020) 219–222, doi:10.3760/cma.j.issn.1001-0939.2020.03.016.

[19] V.K. Maurya, S. Kumar, L. Madan, B. Bhatt, S.K. Saxena, Therapeutic development and drugs for the treatment of COVID-19, in: Coronavirus Disease 2019 (COVID- 19): Epidemiology, Pathogenesis, Diagnosis, and Therapeutics, Springer, Singapore, 2020, pp. 109–126, doi:10.1007/978-981-15-4814-7_10.

[20] P.I. Andersen, A. Ianevski, H. Lysvand, A. Vitkauskiene, V. Oksenych, M. Bjørås, K. Telling, I. Lutsar, U. Dumpis, Y. Irie, T. Tenson, T. Kantele, D.E. Kainov, Discovery and development of safe-in-man broad-spectrum antiviral agents, Int. J. Infect. Dis. 93 (2020) 268–276, doi:10.1016/j.ijid.2020.02.018.

[21] A. Citarella, A. Scala, A. Piperno, N. Micale, SARS-CoV-2 Mpro: a potential target for peptidomimetics and small-molecule inhibitors, Biomolecules 11 (2021) 607–641, doi:10.3390/biom11040607.

[22] A. Sarkar, K. Mandal, Repurposing an antiviral drug against SARS-CoV-2 main protease, Angew. Chem. Int. Ed. Engl. 60 (2021) 23492–23494, doi:10.1002/anie.202107481.

[23] Y. Gupta, S. Kumar, S.E. Zak, K.A. Jones, C. Upadhyay, N. Sharma, S.A. Azizi, R.S. Kathayat, Poonam, A.S. Herbert, R. Durvasula, B.C. Dickinson, J.M. Dye, B. Rathi, P. Kempaiah, Antiviral evaluation of hydroxyethylamine analogs: inhibitors of SARS-CoV-2 main protease (3CLpro), a virtual screening and simulation approach, Bioorg. Med. Chem. 1 (2021) 116393–116404, doi:10.1016/j.bmc.2021.116393.

[24] L. Wen, K. Tang, K.K. Chik, C.C. Chan, J.O. Tsang, R. Liang, J. Cao, Y. Huang, C. Luo, J.P. Cai, Z.W. Ye, F. Yin, H. Chu, D.Y. Jin, K.Y. Yuen, S. Yuan, J.F. Chan, In silico structure-based discovery of a SARS-CoV-2 main protease inhibitor, Int. J. Biol. Sci. 17 (2021) 1555–1564, doi:10.7150/ijbs.59191.

[25] M. Missioui, M.A. Said, G. Demirtas, J.T. Mague, Y. Ramli, Docking of disordered independent molecules of novel crystal structure of (N-(4-methoxyphenyl)-2-(3-methyl-2-oxo-3,4- dihydroquinoxalin-1(2H)-yl)acetamide as anti-COVID-19 and anti-Alzheimer's disease. Crystal structure, HSA/DFT/XRD, J. Mol. Struct. 1247 (2022) 131420, doi:10.1016/j.molstruc.2021.131420.

[26] L.H. Abdel-Rahman, M.T. Basha, B. Saad Al-Farhan, M.R. Shehata, S.K. Mohamed, Y. Ramli, [Cu(dipicolinoylamide)(NO3)(H2O)] as anti-COVID-19 and antibacterial drug candidate: design, synthesis, crystal structure, DFT and molecular docking, J. Mol. Struct. 1247 (2022) 131348, doi:10.1016/j.molstruc.2021.131348.

[27] M. Missioui, M.A. Said, G. Demirtas, J.T. Mague, A. Al-Sulami, N.S. Al-Kaff, Y. Ramli, A possible potential COVID-19 drug candidate:diethyl 2-(2-(2-(3-methyl-2-oxoquinoxalin-1(2H)-yl)acetyl)hydrazono)malonate: docking of disordered independent molecules of a novel crystal structure, HSA/DFT/XRD and cytotoxicity, Arab. J. Chem. 15 (2022) 103595, doi:10.1016/j.arabjc.2021.103595.

[28] (a) M. Berredjem, J.Y. Winum, L. Toupet, O. Masmoudi, N.E. Aouf, J.L. Montero, N-chlorosulfonyloxazolidin-2-ones: synthesis, structure, and reactivity toward aminoesters, Synth. Commun. 34 (2006) 1653–1662, doi:10.1081/SCC-120030753; (b) M. Berredjem, Z. Regainia, G. Dewynter, J.L. Montero, N.E. Aouf, Simple and efficient synthesis of new chiral N, N'-sulfonyl bis-oxazolidin-2-ones, Heteroat. Chem. 17 (2006) 61–65, doi:10.1002/hc.20183; (c) A. Bouzina, I. Grib, K. Bechlem, B. Belhani, N.E. Aouf, M. Berredjem, Efficient synthesis of novel N-acylsulfonamide oxazolidin-2-ones derivatives, Karbala Int. J. Mod. Sci. 2 (2016) 98–103, doi:10.1016/j.kijoms.2016.02.003.

[29] M.C. Burla, R. Caliandro, M. Camalli, B. Carrozzini, G.L. Cascarano, L. De Caro, C. Giacovazzo, G. Polidori, R. Spagna, SIR2004: an improved tool for crystal structure determination and refinement, J. Appl. Cryst. 38 (2005) 381–388, doi:10.1107/S002188980403225X.

[30] G.M. Sheldrick, A short history of SHELX, Acta Cryst. A 64 (2008) 112–122, doi:10.1107/S0108767307043930.

[31] L.J. Farrugia, WinGX and ORTEP for windows: an update, J. Appl. Cryst. 45 (2012) 849–854, doi:10.1107/S0021889812029111.

[32] G.M. Sheldrick, SADABS, Bruker AXS Inc., Madison, Wisconsin, USA, 2002.

[33] A. Douangamath, D. Fearon, P. Gehrtz, T. Krojer, P. Lukacik, C.D. Owen, E. Resnick, C. Strain-Damerell, A. Aimon, P. Ábrányi-Balogh, J. Brandão-Neto, A. Carbery, G. Davison, A. Dias, T.D. Downes, L. Dunnett, M. Fairhead, J.D. Firth, S.P. Jones, A. Keeley, G.M. Keserü, H.F. Klein, M.P. Martin, M.E.M. Noble, P. O'Brien, A. Powell, R.N. Reddi, R. Skyner, M. Snee, M.J. Waring, C. Wild, N. London, F. von Delft, M.A. Walsh, Crystallographic and electrophilic fragment screening of the SARS-CoV-2 main protease, Nat. Commun. 11 (2020) 5047–5058, doi:10.1038/s41467-020-18709-w.

[34] S. Release, 2 (2015) LigPrep, Version 3.4, Schrödinger, LLC, New York, NY, 2015.

[35] R.A. Friesner, J.L. Banks, R.B. Murphy, T.A. Halgren, J.J. Klicic, D.T. Mainz, M.P. Repasky, E.H. Knoll, D.E. Shaw, M. Shelley, J.K. Perry, P. Francis, P.S. Shenkin, Glide: a new approach for rapid, accurate docking and scoring.

1.Method and assessment of docking accuracy, J. Med. Chem. 47 (2004) 1739–1749, doi:10.1021/jm0306430.

[36] R.A. Friesner, R.B. Murphy, M.P. Repasky, L.L. Frye, J.R. Greenwood, T.A. Halgren, D.T. Mainz, Extra precision glide: docking and scoring incorporating a model of hydrophobic enclosure for protein-ligand complexes, J. Med. Chem. 49 (2006) 6177–6196, doi:10.1021/jm0512560.

[37] A.D. Becke, Density-functional thermochemistry. III. The role of exact exchange, J. Chem. Phys. 98 (1993) 5648–5652, doi:10.1063/1.464913.

[38] M.M. Francl, W.J. Pietro, W.J. Hehre, J.S. Binkley, M.S. Gordon, D.J. DeFrees, J.A. Pople, Self-consistent molecular orbital methods. XXIII. A polarization-type basis set for second-row elements, J. Chem. Phys. 77 (1982) 3654–3665, doi:10.1063/1.444267.

[39] M.J. Frisch, G.W. Trucks, H.B. Schlegel, G.E. Scuseria, M.A. Robb, J.R. Cheeseman, et al., Gaussian 09, Revision A.02, 34, Gaussian Inc Wallingford CT, Wallingford CT, 2009.

[40] M. Szafran, A. Komasa, E. Bartoszak-Adamska, Crystal and molecular structure of 4-carboxypiperidinium chloride (4-piperidinecarboxylic acid hydrochloride), J. Mol. Struct. 827 (2007) 101–107, doi:10.1016/j.molstruc.2006.05.012.

[41] K. Bechlem, M. Aissaoui, B. Belhani, K.O. Rachedi, S. Bouacida, R. Bahadi, S.E. Djouad, R. Ben Mansour, M. Bouaziz, F. Almalki, T. Ben Hadda, M. Berredjem, Synthesis, X-ray crystallographic study and molecular docking of new α-sulfamidophosphonates: POM analyses of their cytotoxic activity, J. Mol. Struct. 1210 (2020) 127990–127998, doi:10.1016/j.molstruc.2020.127990.

[42] (a) R.T. Simons, G.E. Scott, A.G. Kanegusuku, J.L. Roizen, Photochemically mediated nickel-catalyzed synthesis of N–(Hetero)aryl sulfamides, J. Org. Chem. 85 (2020) 6380–6391, doi:10.1021/acs.joc.0c00139; (b) A. Bouzina, K. Bechlem, H. Berredjem, B. Belhani, I. Becheker, J. Lebreton, M. Le Borgne, Z. Bouaziz, C. Marminon, M. Berredjem, Synthesis, spectroscopic characterization, and in vitro antibacterial evaluation of novel sulfamidocarbonyloxyphosphonates, Molecules 23 (2018) 1682–1696, doi:10.3390/molecules23071682; (c) J.J. Jun, X.Q. Xie, Implementation of diverse synthetic and strategic approaches to biologically active sulfamides, ChemistrySelect. 6 (2021) 430–469, doi:10.1002/slct.202004765.

[43] (a) K.A. Scott, J.T. Njardarson, Analysis of US FDA-approved drugs containing sulfur atoms, Top. Curr. Chem. 5 (2018) 376–400, doi:10.1007/s41061-018-0184-5; (b) R.G. Gentles, M. Ding, J.A. Bender, C.P. Bergstrom, K. Grant-Young, P. Hewawasam, T. Hudyma, S. Martin, et al., Discovery and preclinical characterization of the cyclopropylindolobenzazepine BMS-791325, a potent allosteric inhibitor of the hepatitis C virus NS5B polymerase, J. Med. Chem. 57 (2014) 1855–1879, doi:10.1021/jm4016894.

[44] (a) M. Berredjem, Z. Regaïnia, A. Djahoudi, N.E. Aouf, G. Dewynter, J.L. Montero, Synthèse Et cyclisation de carboxylsulfamides dérivés d'amines Et d'α-Hydroxyesters. Éavaluation De L'Activité Bactéeriostatique, Phosphorus Sulfur Silicon Relat. Elem. 165 (2000) 249–264, doi:10.1080/10426500008076344; (b) H. Cheloufi, M. Berredjem, W. Boufas, F. Bouchareb, A. Djahoudi, N.E. Aouf, Efficient synthesis, characterization, and antibacterial activity of novel N-acylsulfonamides and sulfonylureas, Phosphorus Sulfur Silicon Relat. Elem. 189 (2014) 1396–1404, doi:10.1080/10426507.2013.865125; (c) R. Bouasla, M. Berredjem, N.E. Aouf, C. Barbey, 1, 2, 3, 4-Tetrahydroisoquinoline-2-sulfonamide, Acta Crystallogr. E Struct. Rep. Online 64 (2008) o432, doi:10.1107/S1600536807068158.

[45] M.C. Etter, Encoding and decoding hydrogen-bond patterns of organic compounds, Acc. Chem. Res. 23 (1990) 120–126, doi:10.1021/ar00172a005.

[46] S. Hari, In silico molecular docking and ADME/T analysis of plant compounds against IL17A and IL18 targets in gouty arthritis, J. Appl. Pharm. Sci. 9 (2019) 18–26, doi:10.7324/JAPS.2019.90703.

[47] F. Ntie-Kang, L.L. Lifongo, J.A. Mbah, L.C.O. Owono, E. Megnassan, L.M. Mbaze, P.N. Judson, W. Sippl, A.M.N. Efange, In silico drug metabolism and pharmacokinetic profiles of natural products from medicinal plants in the Congo basin, In Silico Pharmacol. 1 (2013) 12–23 10.1186%2F2193-9616-1-12.

[48] C.A. Lipinski, Lead- and drug-like compounds: the rule-of-five revolution, Drug Discov. Today Technol. 1 (2004) 337–341, doi:10.1016/j.ddtec.2004.11.007.

[49] C.A. Lipinski, F. Lombardo, B.W. Dominy, P.J. Feeney, Experimental and computational approaches to estimate solubility and permeability in drug discovery and development settings, Adv. Drug Deliv. Rev. 23 (1997) 3–25, doi:10.1016/S0169-409X(96)00423-1.

[50] I. Muegge, S.L. Heald, D. Brittelli, Simple selection criteria for drug-like chemical matter, J. Med. Chem. 44 (2001) 1841–1846, doi:10.1021/jm015507e.

[51] W.J. Egan, K.M. Merz, J.J. Baldwin, Prediction of drug absorption using multivariate statistics, J. Med. Chem. 43 (2000) 3867–3877, doi:10.1021/jm000292e.

[52] A.K. Ghose, V.N. Viswanadhan, J.J. Wendoloski, A knowledge-based approach in designing combinatorial or medicinal chemistry libraries for drug discovery. 1. A qualitative and quantitative characterization of known drug databases, J. Comb. Chem. 1 (1999) 55–68, doi:10.1021/cc9800071.